Biochimica et Biophysica Acta 1807 (2011) 108–118

Contents lists available at ScienceDirect

Biochimica et Biophysica Acta

journal homepage: www.elsevier.com/locate/bbabio

Short circuiting a sulfite oxidising enzyme with direct electrochemistry: Active site substitutions and their effect on catalysis and electron transfer

Trevor D. Rapson [a], Ulrike Kappler [a], Graeme R. Hanson [b], Paul V. Bernhardt [a,*]

[a] Centre for Metals in Biology, School of Chemistry and Molecular Biosciences, University of Queensland, Brisbane, 4072, Australia
[b] Centre for Advanced Imaging, University of Queensland, Brisbane, 4072, Australia

ARTICLE INFO

Article history:
Received 14 July 2010
Received in revised form 6 September 2010
Accepted 15 September 2010
Available online 20 September 2010

Keywords:
Molybdenum
Enzyme
Voltammetry

ABSTRACT

Sulfite dehydrogenase (SDH) from *Starkeya novella* is a heterodimeric enzyme comprising a Mo active site and a heme *c* electron relay, which mediates electron transfer from the Mo cofactor to cytochrome *c* following sulfite oxidation. Studies on the wild type enzyme (SDH^{WT}) and its variants have identified key amino acids at the active site, specifically Arg-55 and His-57. We report the $Mo^{VI/V}$, $Mo^{V/IV}$ and $Fe^{III/II}$ (heme) redox potentials of the variants SDH^{R55K}, SDH^{R55M}, SDH^{R55Q} and SDH^{H57A} in comparison with those of SDH^{WT}. For SDH^{R55M}, SDH^{R55Q} and SDH^{H57A} the heme potentials are lowered from *ca.* 240 mV in SDH^{WT} to *ca.* 200 mV, while the heme potential in SDH^{R55K} remains unchanged and the Mo redox potentials are not affected significantly in any of these variants. Protein film voltammetry reveals a pH dependence of the electrochemical catalytic half-wave potential (E_{cat}) of −59 mV/pH in SDH^{WT} and SDH^{R55K} which tracks the pH dependence of the $Mo^{VI/V}$ redox potential. By contrast, the catalytic potentials for SDH^{R55M} and SDH^{H57A} are pH-independent and follow the potential of the heme cofactor. These results highlight a switch in the pathway of electron exchange as a function of applied potential that is revealed by protein film voltammetry where an actuation of rate limiting intramolecular electron transfer (IET, Mo to heme) at high potential attenuates the catalytic current relative to faster, direct electron transfer (Mo to electrode) at lower potential. The same change in electron transfer pathway is linked to an unusual peak-shaped profile of the ideally sigmoidal steady state voltammogram in SDH^{WT} alone, which has been associated with a potential dependent change in the orientation of the enzyme on the electrode surface. All other variants show purely sigmoidal voltammetry due to their inherently slower turnover numbers which are always lower than IET rates.

1. Introduction

Sulfite oxidising enzymes are found in all living organisms and catalyse the oxidation of sulfite to sulfate thereby preventing cellular damage by reactive sulfite species [1]. All known sulfite oxidising enzymes share an active site comprising a five-coordinate Mo ion coordinated to a bidentate dithiolene molybdopterin ligand, a Cys residue and a pair of *cis* oxo ligands when the enzyme is in its fully oxidised Mo^{VI} form (Scheme 1) [2–4]. Like all other mononuclear Mo enzymes [5,6], the active site metal cycles between its Mo^{IV} and Mo^{VI} oxidation states during catalysis while performing the 2-electron, O-atom transfer conversion of sulfite to sulfate where the equatorial oxo ligand of the Mo^{VI} form is transferred to sulfite. Given their redox activity, mononuclear Mo enzymes have emerged as an exciting field for enzyme biosensor development given their generally high substrate specificity and increasing availability [7].

Sulfite oxidising enzymes from vertebrate (human and chicken sulfite oxidase, HSO and CSO) [8], plant (plant sulfite oxidase, or PSO) [9] and bacterial (sulfite dehydrogenase, or SDH) [10,11] sources have been characterised. In addition to nearly identical active site geometries, they all contain the conserved active site residues Cys-104, Tyr-236, His-57 and Arg-55 (Fig. 1, *Starkeya novella* SDH numbering) [3]. Both vertebrate sulfite oxidising enzymes and the bacterial SDH from *S. novella* contain heme groups as accessory redox centers. In the vertebrate enzymes the heme and Mo domains are linked by a flexible loop and catalysis requires a repositioning of the heme domain to allow electron transfer between the heme and Mo domains. In SDH the heme and Mo cofactors are located on separate subunits and the position of these subunits does not change during catalysis [3,8,12]. This simplifies analysis of the catalytic cycle of the enzyme as no protein conformational changes are coupled with electron and atom transfer. This makes SDH an excellent model for mechanistic studies of enzymatic sulfite oxidation. A further advantage is that SDH is amenable to crystallization, the crystal structures for the wild type enzyme in addition to SDH^{Y236F}, SDH^{R55M} and

Abbreviations: EDTA, ethylenediamine tetraacetate; EPR, electron paramagnetic resonance; NHE, normal hydrogen electrode; SDH, sulfite dehydrogenase; CSO, chicken sulfite oxidase; HSO, human sulfite oxidase

* Corresponding author.
E-mail address: p.bernhardt@uq.edu.au (P.V. Bernhardt).

0005-2728/$ – see front matter © 2010 Elsevier B.V. All rights reserved.
doi:10.1016/j.bbabio.2010.09.005

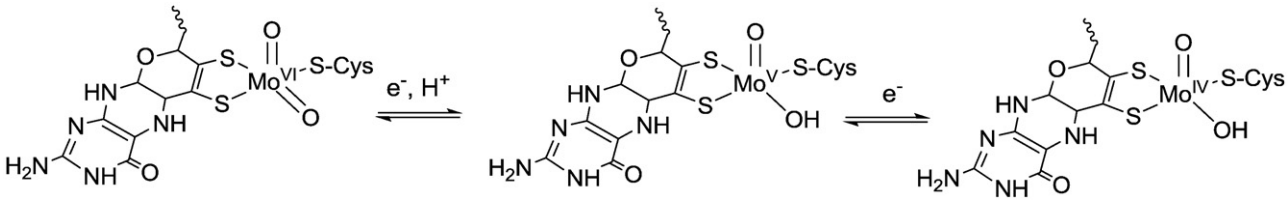

Scheme 1. Proton coupled redox reactions of the SDH active site.

SDH^{H57A} have been reported [13,14] while crystal structures are not yet available for human sulfite oxidase.

The roles of the conserved residues Arg-55, His-57 and Try-236 in enzymatic sulfite oxidation have been recently reported [13,15]. Arg-55 is intimately involved in H-bonding (Fig. 1) and all three N-atoms of the guanidinium moiety donate H-bonds to neighboring groups. The secondary N-atom of Arg-55 is an H-bond donor to the equatorial Mo-oxo/hydroxo ligand (Mo^{VI}=O or Mo^{V}–OH) and this sidechain also donates H-bonds *via* both primary N-atoms to heme propionate-6. The Arg-55 sidechain has been shown to mediate substrate binding and product release [13]. Tyr-236 was found to be important in enzymatic turnover and stability of the Mo cofactor [14], while a His-57 substitution, although not directly linked to the Mo center, led to a decrease in substrate affinity at low pH and disorder in the position of Arg-55 apparent in both the crystal structure and EPR studies [13]. The imidazole ring of His-57 is in H-bonding proximity to both Tyr-236 (Fig. 1) and to the carbonyl O-atom of the molybdopterin group (oriented to the rear in Fig. 1).

Protein film voltammetry (PFV), where a protein is immobilized on an electrode and catalysis is observed directly (without mediators) as a function of applied potential is a powerful tool in investigating the catalytic properties of oxido-reductase enzymes [16–18]. In previous PFV studies on wild type sulfite dehydrogenase (SDH^{WT}) from *S. novella* we identified optimized experimental conditions that enabled the investigation of substrate and inhibitor concentrations on catalysis [19,20]. An unusual substrate dependence was noted for the voltammetric response where an apparent 'potential optimum' was reached beyond which catalysis was slowed [20]. Normally one expects catalysis to reach a plateau once the redox potentials of all cofactors are traversed, consistent with an enzyme limited steady state. A similar PFV investigation on CSO published by Elliott et al. did not reveal such behavior [21]. In order to better understand the unusual voltammetric effects we have seen in SDH^{WT}, three variants bearing substitutions of Arg-55, which occupies a crucial position between the Mo and heme cofactors (Fig. 1), have been characterized. These variants are SDH^{R55K} (where the positive charge of the side chain is conserved), SDH^{R55Q} (equivalent to the HSO mutation which causes fatal sulfite oxidase deficiency) and SDH^{R55M} (a hydrophobic substitution which retains similar steric properties to the native enzyme). The crystal structure of SDH^{R55M} showed [13] that the thioether sidechain of Met-55 does not occupy the same position as the guanidinium group of Arg-55. Instead, the Met-55 side chain is oriented away from the active site leaving the position previously occupied by the Arg-55 guanidinium group vacant [13]. Another active site substituted enzyme SDH^{H57A} has also been investigated in this study given the changes noted above in substrate binding and catalytic activity associated with this variant. Our results comprising a combination of protein film voltammetry and redox potentiometry measurements, have enabled us, for the first time, to elucidate the origin of unusual non-ideal peak shaped voltammetry noted in previous studies [19,20] and also to tune the redox potential of the heme cofactor by choice of the amino acid residues at positions-55 and -57, which each play an important role in the rate of catalysis and the pathway of electron transfer.

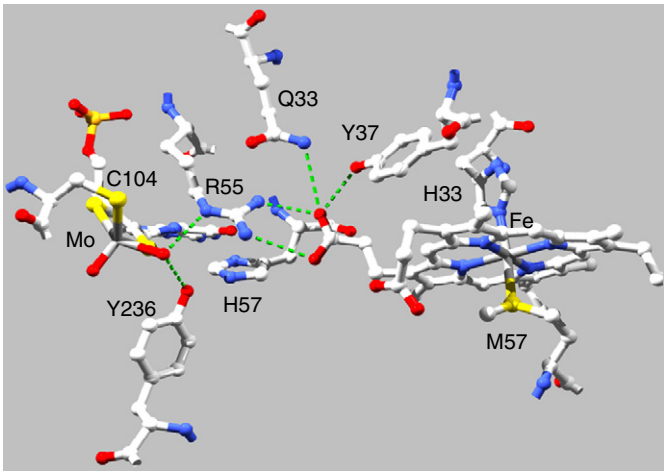

Fig. 1. The active site of SDH^{WT} as determined by X-ray crystallography [3] (coordinates taken from the Protein Data Bank, structure 2BLF) showing the Mo and heme cofactors and active site residues. Structure manipulated with Swiss PDB Viewer (vers. 3.7) and rendered with PovRay (vers. 3.5).

2. Materials and methods

2.1. Materials

The procedure employed to generate substituted enzymes SDH^{R55M}, SDH^{H57A} and SDH^{Y236F} has been described by Bailey et al. [13]. The isolation of SDH^{R55Q} and SDH^{R55K} has also been reported [15]. All recombinant enzymes were produced using a heterologous expression system in *Rhodobacter capsulatus* [22].

All reagents used were of analytical grade purity and used without any further pre-treatment except for Ti^{III} citrate which was prepared as described by Codd et al. [23]. All solutions were prepared in purified water (Millipore, 18.2 MΩ cm^{-1}). A buffer mixture containing both bis-tris propane (10 mM) and 2-amino-2-methylpropan-1-ol (10 mM) was used, titrated with acetic acid to give the desired pH. Sulfite was added from a stock solution, freshly prepared in a solution of tris acetate (50 mM), pH 8.8 with 5 mM EDTA.

2.2. Redox potentiometry

Ti^{III} citrate [23] was employed as the reductant instead of the more commonly used dithionite. Oxidation of dithionite generates sulfite (the enzyme substrate) which initiates further reduction of the enzyme thus making control of the redox potential difficult. $K_2S_2O_8$ (oxidant) was the oxidant and both this and the Ti^{III} citrate were added in microlitre aliquots as *ca.* 1 mM solutions.

The molybdenum and heme redox potentials were determined by EPR and optical potentiometry, respectively. All experiments were carried out inside a Belle Technology glovebox under an atmosphere of N_2 (with O_2<10 ppm) at 25 °C. Potentials were measured using a combination Pt wire and Ag/AgCl reference electrode calibrated against a pH 7 quinhydrone solution (E'(pH 7) +284 mV *vs.* NHE). All potentials have been corrected relative to NHE.

The heme redox potentials were measured using 5 μM enzyme in 20 mM Tris acetate buffer (pH 8.0). The solution potentials were stabilized using the reported [24] high potential Fe complexes as mediators: Fe(NOTA) and $[Fe(tacn)_2]Br_3$ (5 μM of each) (NOTA = 1,4,7-triazacyclononane-triacetate and tacn = 1,4,7-triazacyclononane). Changes in the UV-Vis spectrum of the oxidized and reduced forms of the heme were monitored continuously at 417 nm with an Ocean Optics USB4000 fibre optic spectrometer (with the cell stand mounted inside the glovebox and under continuous stirring). Equilibrium was established when there was no further change in either the optical absorbance (A) or solution potential (E). The midpoint potential (E_m) was determined using Eq. (1) [24] where A_{ox} and A_{red} are the limiting absorbance values of the heme chromophore in its oxidized and reduced forms, respectively at 293 K.

$$A = \frac{A_{ox}10^{\frac{E-E_m}{59}} + A_{red}}{1 + 10^{\frac{E-E_m}{59}}} \quad (1)$$

EPR redox potentiometric titrations were carried out using enzyme concentrations of 15–30 μM (depending on the substituted enzyme studied) in a 50 mM tricine buffer (pH 8.0). The transition metal complexes [Fe(NOTA)], $[Fe(tacn)_2]Br_3$, $[Co((NMe_3)_2sar)]Cl_5$, $[Co((Cl,Me)N_5Ssar)]Cl_3$, $[Co((NH_2,Me)N_4S_2sar)]Cl_3$ and $[Co(sep)]Cl_3$ (each 20 μM, ligand abbreviations defined elsewhere [24]) were used to span the wider potential range necessary to cover the titration from Mo^{VI} to Mo^{IV}. For each EPR spectrum, 100 μL aliquots were withdrawn from the equilibrated solution, transferred to an EPR tube and sealed within the glovebox. Each tube was immediately removed from the glovebox and carefully frozen in liquid N_2 by gradual immersion to avoid fracture of the tube upon expansion of the frozen liquid.

EPR measurements were acquired on a Bruker Elexsys E580 X-band EPR spectrometer at 140 K (modulation amplitude of 2.0 G and microwave power of 10 mW). The intensity of the high g-value Mo^V signal (I) was taken to be proportional to the concentration of Mo^V and fitted to a modified form of the Nernst equation describing consecutive one-electron reductions of a center with redox potentials E_1 and E_2 with a maximum intensity (I_p) [14].

$$I(E) = \frac{I_p}{1 + 10^{(E-E_1)/59} + 10^{(E_2-E)/59}} \quad (2)$$

2.3. Electrochemical measurements and electrode preparation

In general the substituted enzymes were less stable on the electrode than the wild type SDH. In particular, long drying times of concentrated enzyme solutions to give a film on the electrode surface led to a significant lowering of electrocatalytic activity. To overcome this problem, the electrodes were dried at room temperature and small volumes of enzyme were added to the electrode thus reducing evaporation time.

Cyclic voltammetry and chronoamperometry were carried out on a BAS100B/W workstation using a three electrode system of a home-made edge oriented pyrolytic graphite (Le Carbone, Ltd. Sussex, U.K.) working electrode (surface area 0.1 cm^2), platinum wire counter electrode and a Ag/AgCl reference electrode (+196 mV *vs.* NHE). All potentials have been corrected relative to NHE. The electrode was attached to a BAS RDE-3 rotating disk apparatus and rotated at 500 rpm.

The working electrode was prepared as described previously [20] using a microtome to cleave a 1 μm layer from the face of the electrode followed by cleaning using sonication in MilliQ water. The substituted enzymes (2 μL, 25 μM) were co-adsorbed onto the dry graphite electrode with 2 μL solutions of either poly-DL-lysine (hydrobromide) (1 mg/mL, Sigma-Aldrich M.W. 93–124 kDa) or kanamycin (10 mg/mL) and air dried at room temperature for 30 min. Experimental details are provided in the figure legends. Chronoamperometric determinations of catalytic current were carried out as described previously [20].

3. Results

3.1. Protein film voltammetry of SDH^{WT} and its variant forms

The electrochemically driven enzymatic oxidation of sulfite to sulfate is achieved through protein film voltammetry (PFV) and provides a direct measurement of catalysis through the measurement of the anodic current as a function of applied potential. As described in the Materials and methods section, each enzyme for voltammetry was immobilized on the conducting surface of an edge plane-oriented pyrolytic graphite (EPG) electrode as a film (evaporated from a few microlitres of solution). Co-adsorption with non-electroactive compounds such as poly-DL-lysine or kanamycin enhanced the stability of the enzyme film against desorption and this also improved the reproducibility of each experiment. Under these conditions enzyme diffusion is eliminated as all electroactive enzyme molecules are confined to the adsorbed layer at the electrode surface and only substrate diffusion to these enzymes is significant. To also avoid complications from (time-dependent) substrate depletion during the voltammetric sweep, rotating disk voltammetry was employed to ensure that the substrate concentration at the electrode surface was the same as that in the bulk and a true steady state was maintained throughout the sweep. Under these ideal steady state conditions the mechanism of the electrochemically driven reaction is simple and follows Michaelis–Menten kinetics as shown in Scheme 2 where the same rate constants associated with substrate binding and release (k_1 and k_{-1}) and turnover (k_2) are illustrated. The enzyme's physiological electron transfer partner (in this case a c-type cytochrome) [10] is replaced by the electrode.

An example of the typical voltammetric profile of SDH^{WT} is shown in Fig. 2. In the absence of sulfite, no Faradaic current is observed (dotted line) and this serves as a baseline (blank) voltammogram. Redox responses from the Mo and heme cofactors under these conditions are too small to be detected relative to the background charging current. However, in the presence of sulfite, catalysis switches on and the current rises in a Nernstian (sigmoidal) way until a plateau is reached at the point where all enzyme molecules on the electrode surface are maintained in their active form *i.e.* heterogeneous electron transfer (reoxidation of the enzyme at the electrode) occurs faster than either enzymatic sulfite oxidation or substrate diffusion to the enzyme (driven by the rapidly rotating electrode). On the reverse (cathodic) sweep catalysis is switched off again and the current decreases again in a sigmoidal fashion. The anodic and cathodic sweeps are identical when adjusted for the charging current.

Under steady state conditions the maximum catalytic current at high overpotential and saturating concentrations of sulfite (i_{max}) is

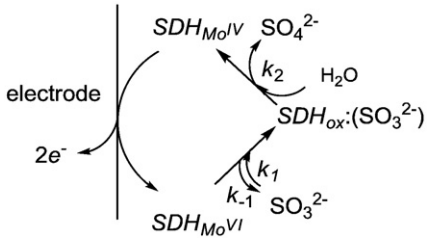

Scheme 2. Definition of kinetic parameters for SDH catalysis.

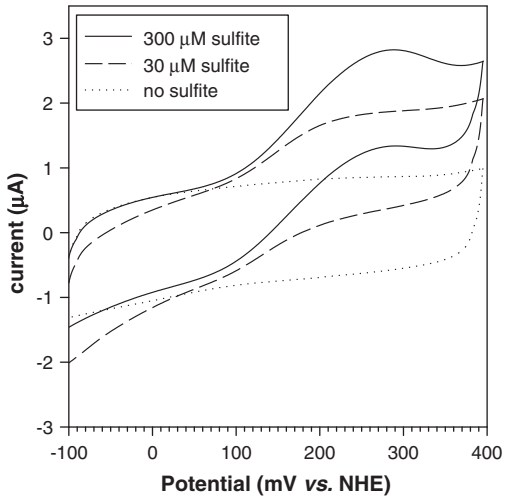

Fig. 2. Rotating disk (500 rpm) cyclic voltammetry of SDH^{WT} at pH 8.0 and adsorbed to a pyrolytic graphite working electrode in the presence of the following sulfite concentrations: 300 μM (———), 30 μM (– – –) and no sulfite (···).

limited only by the enzyme turnover number, k_2 and surface coverage of active enzyme Γ_{SDH} (mol cm^{-2}) (Eq. (3))

$$i_{max} = nFA\Gamma_{SDH} \times k_2 \tag{3}$$

where F is the Faraday constant, A the electrode area (cm^2) and n is the electron stoichiometry (in this case 2). At lower sulfite concentrations, the limiting current (i_{lim}) follows Michaelis–Menten kinetics (Eq. (4)) characterized by an electrochemical Michaelis constant $K_{M,echem}$ [25,26].

$$i_{lim} = \frac{nFA\Gamma_{SDH}k_2\left[SO_3^{2-}\right]}{K_{M,echem} + \left[SO_3^{2-}\right]} \quad \text{where } K_{M,echem} = \frac{k_2 + k_{-1}}{k_1} \tag{4}$$

3.2. pH dependence of the electrochemical Michealis constant ($K_{M,echem}$)

To ensure that catalytic function was not impaired by adsorption of the enzyme on the electrode, the pH dependency of the electrochemically determined Michaelis constants ($K_{M,echem}$) of all enzymes were determined and compared with data obtained from solution assays using cytochrome *c* as an electron acceptor [12]. In each case, the steady state catalytic current (i_{lim}) at 300 mV *vs.* NHE was measured as a function of sulfite and the data fit to Eq. (4). At a potential of 300 mV *vs.* NHE direct, non-specific sulfite oxidation at the electrode is negligible. No significant catalytic responses were obtained for SDH^{R55Q} as expected from its known poor activity in solution assays relative to SDH^{WT} ($K_{M\ soln}$ for SDH^{R55Q} = 2250 μM *vs.* 0.6 μM for SDH^{WT} at pH 6) [15].

Sulfite oxidising enzymes all show a characteristic high affinity for sulfite at low pH which generally decreases at more alkaline pH. All enzymes in Fig. 3 follow this trend. For SDH^{R55K} an approximately five fold increase in $K_{M,echem}$ was obtained relative to SDH^{WT} at pH 8. However, a more pronounced 1–2 orders of magnitude increase in $K_{M,echem}$ was seen for the SDH^{R55M} variant relative to SDH^{WT} (note change of scale on right hand axis of Fig. 3). These changes are similar to those found in solution assays for the corresponding enzymes [13,15]. A notable exception to this trend is SDH^{H57A} (Fig. 4) where the $K_{M,echem}$ values exhibit a minimum at about pH 7, which also mirrors behavior observed in solution assays of SDH^{H57A} ($K_{M\ soln}$ for SDH^{H57A} = 667 μM at pH 6 and 270 μM at pH 8) [13].

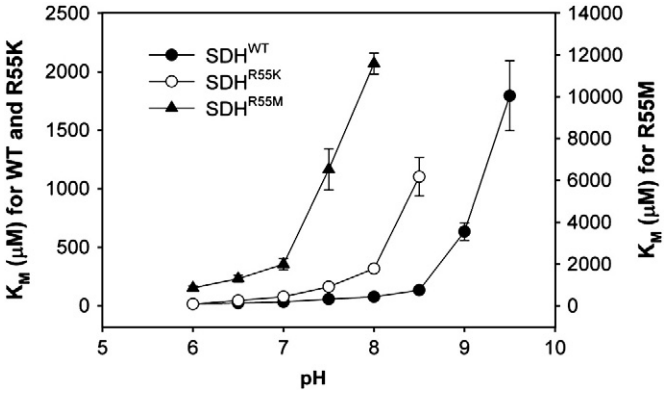

Fig. 3. The pH dependence of $K_{M,echem}$ (sulfite) for SDH^{WT}, SDH^{R55M} and SDH^{R55K} (note change of scale for SDH^{R55M}). Each enzyme was immobilized in a polylysine film on an EPG electrode rotated at 500 rpm.

3.3. pH dependence of the electrochemical reaction velocity (i_{max})

The rate of electrochemically driven SDH catalysis is also pH dependent. The optimal pH values for catalysis by SDH^{WT}, SDH^{R55K}, SDH^{R55M} and SDH^{H57A} were determined (Fig. 5) by measuring the limiting voltammetric current at 300 mV *vs.* NHE in the presence of a saturating concentration of sulfite (2 mM). The maximum catalytic current (i_{max}) in each system is directly proportional to the (pH dependent) electrochemical turnover number (k_2, see Eq. (3)).[1]

For SDH^{WT}, SDH^{H57A} and SDH^{R55K} (Fig. 5), the experimental data were characteristic of an amphiprotic active site that is deactivated by a protonation (pK_{a1}) or deprotonation (pK_{a2}): SDH^{WT} (pK_{a1} 6.3 and pK_{a2} 8.9); SDH^{H57A} (pK_{a1} 5.9 and pK_{a2} 8.6) and SDH^{R55K} (pK_{a1} 7.0 and pK_{a2} 8.3). The data were modelled with Eq. (5) [27].

$$i_{lim}(pH) = \frac{i_{opt}}{1 + 10^{(pH - pK_{a1})} + 10^{(pK_{a2} - pH)}} \tag{5}$$

For SDH^{R55M} only a single pK_a (7.1) was determined on the basic limb of the profile. The apparent pH optimum was unusually low (<pH 6) and an accurate value for pH_{opt} was not reached within the pH range investigated. However, this result should be viewed with caution as it is possibly due to an artefact of the experimental conditions. Substrate concentrations of 2 mM sulfite were used for SDH^{R55M}. Due to its very large $K_{M,echem}$ value at pH 8, SDH^{R55M} is not saturated with substrate at the higher pH range (see Fig. 3). Therefore the 'limiting' currents plotted in Fig. 5 for SDH^{R55M} (>pH 8) are probably underestimated, higher sulfite concentrations were avoided due to problems of direct sulfite oxidation interference and substrate inhibition. A similar effect was noted in solution assays [13].

The similarity between the electrochemically determined kinetic parameters presented here and data obtained from solution assays indicates that native enzymatic activity of SDH^{WT} and its variants has been maintained and that adsorption of the enzyme on an electrode has not led to any identifiable adverse effects such as denaturation or loss of activity in any way. Also it is relevant that the amino acid substitutions are internal and do not affect the surface charges of the protein so we expect that interactions with the co-adsorbate poly-L-lysine are conserved across the series.

[1] The absolute values of limiting currents from one enzyme to the next cannot be compared as they are each proportional to the surface coverage of enzyme in each experiment (Γ_{SDH}) which is unknown. However, pK_a and pH_{opt} values can be determined assuming Γ_{SDH} is constant throughout each pH dependent experiment.

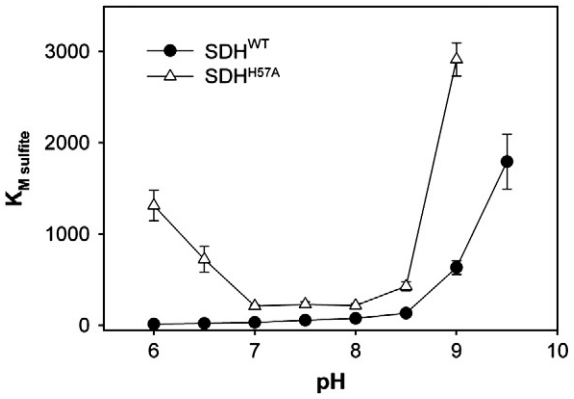

Fig. 4. The pH dependence of $K_{M,echem}$ (sulfite) values for SDH^{H57A} compared to SDH^{WT}. Each enzyme was immobilized in a polylysine film on an EPG with an electrode rotation rate of 500 rpm.

3.4. pH dependence of the catalytic potential (E_{cat})

Protein film voltammetry allows the potential at which catalysis occurs to be measured, which is not possible with traditional solution assays. The catalytic operating potential relates to the minimum thermodynamic driving force needed to facilitate catalysis and may be significantly lower than the redox potential of the native electron partner.

The catalytic half-wave potentials (E_{cat}) were determined from the voltammograms where their second derivative is zero [25,26,28], which is more accurate than extracting data from an inflection point on a normal voltammogram. We have previously reported a strong pH dependence of the E_{cat} values for SDH^{WT} at saturating sulfite concentrations (300 μM–3 mM) [19,20] and these data are shown as diamonds in Fig. 6. To investigate the differences between SDH^{WT} and its variants, the effect of pH on E_{cat} was measured at the same saturating sulfite concentrations. SDH^{R55K} was found to have similar pH dependence of E_{cat} as SDH^{WT} (a change of −59 mV/pH unit, inverted triangles in Fig. 6). This pH dependence of E_{cat} is significantly larger than the errors in measuring these values ~10 mV. There was a pronounced departure from this trend in both SDH^{R55M} and SDH^{H57A} (squares and triangles in Fig. 6) where the values of E_{cat} were pH-independent within the range $6<pH<9$.

Studies carried out previously on the effect of pH on the redox potentials in SDH and other sulfite oxidising enzymes have indicated that the Mo$^{VI/V}$ couple is pH dependent, while the heme redox couple is pH-independent [19,29]. The experimental data presented here suggests that E_{cat} for SDH^{WT} and SDH^{R55K} follows the Mo$^{VI/V}$ redox couple while the E_{cat} values for SDH^{R55M} and SDH^{H57A} track the Fe$^{III/II}$

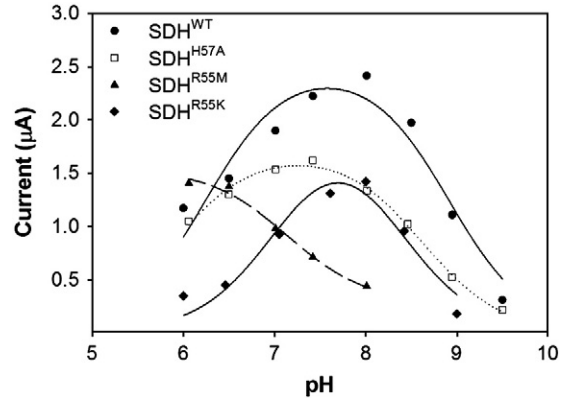

Fig. 5. The pH dependence of catalytic current maximum for sulfite oxidation by SDH^{WT} and substituted forms.

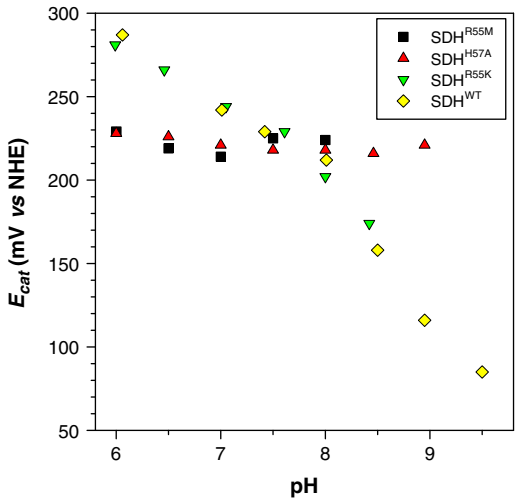

Fig. 6. The pH dependence of the catalytic half-wave potential (E_{cat}) of SDH^{WT} and its substituted forms determined from the second derivative catalytic voltammograms. Saturating concentrations of sulfite were used (SDH^{WT} – 300 μM, SDH^{R55K} and SDH^{H57A} – 600 μM, SDH^{R55M} – 2 mM). The data for SDH^{WT} are taken from ref. [20].

redox potentials; the latter pair being more in keeping with the behaviour of chicken liver SO [21,30].

3.5. Redox potentials of the enzyme cofactors

Very little data on the redox properties of the substituted SDH enzymes was available to substantiate the link between E_{cat} and the redox couple being addressed in the enzyme, so we have determined the Mo and heme redox potentials independently. The Mo$^{VI/V}$ and Mo$^{V/IV}$ redox potentials for SDH^{WT}, SDH^{R55M} and SDH^{H57A} were measured at pH 8 using EPR monitored redox potentiometry (Mo^{V} being the EPR active form). An illustrative example is shown in Fig. 7A for SDH^{H57A} and all data appear in Table 1. Clearly, the Mo$^{VI/V}$ potentials of SDH^{WT}, SDH^{R55M} and SDH^{H57A} are not significantly different (note the experimental uncertainties). The Mo$^{V/IV}$ couples of SDH^{WT}, SDH^{R55M} and SDH^{H57A} appear at about 150–250 mV lower potential.

Given the lack of change determined in the Mo redox potentials, the effect of the same amino acid substitutions on the heme redox couples was determined using UV-vis spectroscopy where the ferric and ferrous forms of the heme are distinctly different and provide an ideal indicator of the degree of reduction. The data were well modelled by Eq. (1) (see Fig. 7B) and the redox potentials are given in Table 1. The heme redox potentials (pH 8) for SDH^{R55M}, SDH^{R55Q} and SDH^{H57A} were *ca.* 40 mV lower than that of SDH^{WT}. The heme potential was unaltered by the SDH^{R55K} substitution. Investigations of the heme redox potentials as a function of pH could not be undertaken with the amounts of the variant forms available. Unlike SDH^{WT}, which can be expressed with high yields, over-expression of the substituted enzymes gave rise to only 10–20% of the yields obtainable for SDH^{WT}; insufficient to permit a complete pH dependent analysis of their redox potentials.

The SDH^{R55K} and SDH^{R55Q} variants were not available in sufficient quantities to study by EPR potentiometry as each titration requires 5–10 mg of protein. Alternatively laser flash photolysis experiments described in detail elsewhere [15,31] allow the Mo$^{VI/V}$ couple to be determined indirectly as long as the Fe$^{III/II}$ potential is known. Briefly, starting with the fully oxidized enzyme (Mo^{VI}:Fe^{III}) reduction with photoexcited deazariboflavin (dRF*) generates a nonequilibrium mixture of the two redox isomers Mo^{V}:Fe^{III} and Mo^{VI}:Fe^{II} (Scheme 3). Time resolved optical spectroscopy reveals the rate at which equilibrium is established (k_{obs}, Eq. (6a)) and the position of this equilibrium (K_{eq}, based on the heme chromophore absorption)

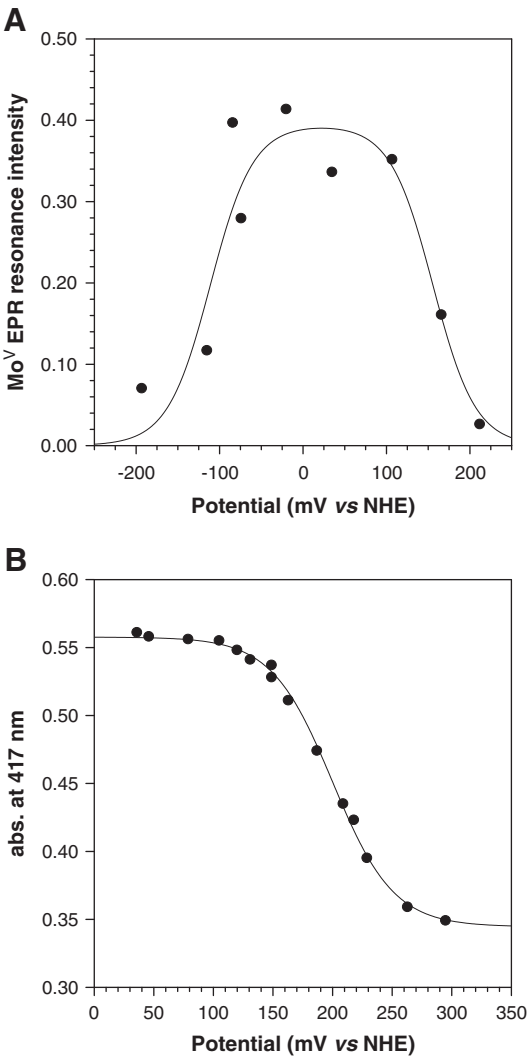

Fig. 7. Redox titrations for SDH^{H57A} showing (A) the Mo^{V} EPR signal intensity (arbitrary units) and (B) the ferrous heme optical absorbance maximum at 417 nm, each as a function of redox potential. The curves show fits to the experimental data points (filled circles) using Eqs. (2) and (1), respectively.

[15,31–35] (Eq. (6b)). The Mo$^{VI/V}$ redox potential is obtained from K_{eq} and the heme redox potential (Eq. (7)).

$$k_{obs} = k_f + k_r \tag{6a}$$

$$K_{eq} = k_f / k_r \tag{6b}$$

$$K_{eq} = e^{(E_{Mo(VI/V} - E_{Fe(III/II)})F/RT} \tag{7}$$

Table 1
Redox potentials (mV *vs.* NHE) of wild type SDH and variants at pH 8. Values in italics calculated from laser flash photolysis data reported previously [15] and Eq. (7) using the Fe$^{III/II}$ potentials in the right hand column and extrapolated from pH 6 on the basis of a single electron, single proton coupled reaction (a −59 mV/pH variation in potential). The uncertainties are assumed to propagate from the heme potentials.

	Mo$^{VI/V}$	Mo$^{V/IV}$	Fe$^{III/II}$
SDH^{WT}	+172±20	+31±20	+242±7
SDH^{H57A}	+154±20	−113±20	+200±4
SDH^{R55M}	+173±20	−86±20	+191±2
SDH^{R55Q}	*+57±2*		+197±2
SDH^{R55K}	*+61±3*		+236±3

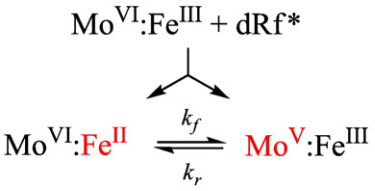

Scheme 3. Flash photolysis reduction of fully oxidized SDH with deazariboflavin (dRF*).

In order to ensure that the (pH dependent) Mo$^{VI/V}$ redox potential (see Scheme 1) is sufficiently high that Fe^{II}→Mo^{V} IET is measurable (k_f>0, Scheme 3), flash photolysis experiments are typically conducted at low pH (5–6). The single electron proton coupled reduction of O Mo^{VI} to HO–Mo^{V} leads to an obligate −59 mV/pH variation in the redox potential within the range 6<pH<9 (where no pK_a is found for either the O Mo^{VI} or HO–Mo^{V} moieties), so the Mo$^{VI/V}$ potential determined at low pH may be extrapolated easily to pH 8. In SDH^{R55M} and the catalytically inactive SDH^{R55Q} variant [15] the calculated Mo$^{VI/V}$ potential at pH 8 is somewhat lower than found in SDH^{WT}, SDH^{R55M} and SDH^{H57A} (Table 1). This difference should be viewed with caution as one is comparing an experimentally determined value with a calculated value.

4. Discussion

4.1. Influence of active site substitutions on the cofactor redox potentials

The Mo$^{VI/V}$ redox potentials (pH 8, Table 1) of SDH^{WT}, SDH^{H57A} and SDH^{R55M} do not differ significantly (considering their experimental uncertainties). The most significant changes were seen in the heme redox potentials which were determined to a greater precision. The Fe$^{III/II}$ redox potentials of SDH^{WT} and SDH^{R55K} were the same within experimental error and 40–50 mV higher than the heme potentials of SDH^{R55M}, SDH^{R55Q} and SDH^{H57A} (Table 1). All of the SDH heme potentials are more than 100 mV higher than in chicken liver SO [21,29].

X-ray crystallography of SDH^{WT} has shown [3] that the guanidinium group of Arg-55 forms a bidentate H-bonding interaction with one of the heme propionates (Fig. 1). The conservative substitution SDH^{R55K} preserves this positive charge and H-bonding capability. In SDH^{R55M} and SDH^{R55Q} the positive charge is lost, uncompensated by the thioether (methionine) or primary amide (glutamine) side chains. This illustrates that a positive charge in position-55 plays a dominant role in regulating the heme redox potential.

A similar decrease of *ca.* 40 mV was also noted for the heme redox potential of SDH^{H57A} compared to the wild type enzyme (Table 1), yet Arg-55 is still conserved. X-ray crystallography has shown that the imidazole side chain of His-57 plays an important structural role in stabilising the position of the Arg-55 residue [13]. In SDH^{H57A} the guanidinium sidechain is displaced away from its usual location, in H-bonding contact with the heme propionate. The loss of this positively charged group at position-55 results in a similar lowering of the heme redox potential seen in SDH^{R55Q} and SDH^{R55M}, albeit by a different mechanism.

4.2. pH dependence of E_{cat}: actuation of different electron transfer pathways

This paper presents the direct electrochemistry of a number of substituted SDH enzymes. Using direct electrochemistry is possible to determine the catalytic potential, E_{cat}. The ability to do so is a major advantage of PFV techniques over other methods where indirect (mediated) electron transfer is measured where the catalytic potential is masked by the mediator. Such indirect electrochemical investigations employing eukaryotic sulfite oxidases (CSO and HSO)

coupled with either small molecular weight coordination compounds or cytochrome *c* as the electron transfer mediator have been reported [36–42].

In this study the pH dependence of E_{cat} in SDH^{WT} and SDH^{R55K} is in stark contrast to that of SDH^{R55M} and SDH^{H57A} (Fig. 6). Studies carried out on sulfite oxidising enzymes by ourselves and others have indicated that the $Mo^{VI/V}$ couple varies by −59 mV/pH, while the $Fe^{III/II}$ couple is pH-independent [19,21,29]. It appears that the E_{cat} values of SDH^{WT} and SDH^{R55K} show a similar pH dependence to that of the $Mo^{VI/V}$ redox couple, while the E_{cat} values for SDH^{R55M} and SDH^{H57A} are similar to that of the Fe redox couples.

These contrasting E_{cat} data and their correspondence with the independently determined redox potentials of the Mo and heme cofactors indicate thermodynamic control of the electron transfer pathway whereby the catalytic electrochemical potential (and its pH dependence) tracks that of the preferred (lower potential) redox couple (either $Mo^{VI/V}$ or $Fe^{III/II}$ depending on the enzyme). The heme cofactor is the known site of electron exchange with the physiological electron partner cytochrome *c* but in protein film voltammetry there is no obvious specific interaction between the electrode and the enzyme that favours either the Mo or heme subunits. In the case of SDH^{WT} and SDH^{R55K} on thermodynamic grounds (70–170 mV lower redox potential) Mo becomes the electron donor rather than Fe. In other words the enzyme has been short-circuited and the heme is bypassed. In the case for SDH^{R55M} and SDH^{H57A}, the amino acid substitutions in the vicinity of the heme propionate lower the heme redox potential to the point where it is the heme group becomes the preferred site of heterogeneous electron transfer (*via* the Mo active site).

4.3. Modelling the peak-shaped voltammetry

A distinct difference was noted in the catalytic waveform of SDH^{WT} (Fig. 8A) compared to that of SDH^{R55K}, SDH^{H57A} and SDH^{R55M} (Fig. 8B–D). SDH^{WT} had a peak shaped waveform which is lost in all the other cases. In the case of SDH^{H57A} and SDH^{R55M} where higher sulfite concentrations were employed, direct sulfite oxidation can be seen at ~350 mV (Fig. 8C and D). These differences are both significant and of great interest. When substrate delivery to the active site is fast and heterogeneous electron transfer is rapid an ideally sigmoidal (steady state) voltammogram is expected [18,25,43]. In the simplest case where there is only one redox center (the active site) the catalytic potential corresponds to that of the active site. In more complex multi-centered enzymes the situation is not as straightforward as intramolecular electron transfer (IET) rates between relay centers need to be considered as discussed in detail elsewhere [44].

We have already demonstrated that the peak-shaped voltammograms in Fig. 8A are not a result of substrate depletion (transient behavior) as the same profile is obtained on the reverse (cathodic) sweep (see Fig. 2) and the waveform does not change as the electrode rotation rate is increased [20]. Product (sulfate) inhibition has been investigated previously [20] and shown to be insignificant; particularly under hydrodynamic conditions where sulfate is rapidly removed from the reaction layer near the electrode surface. The peak shaped features are also present at other pH values [20] so rate limiting proton transfer cannot be responsible for the lowering of activity.

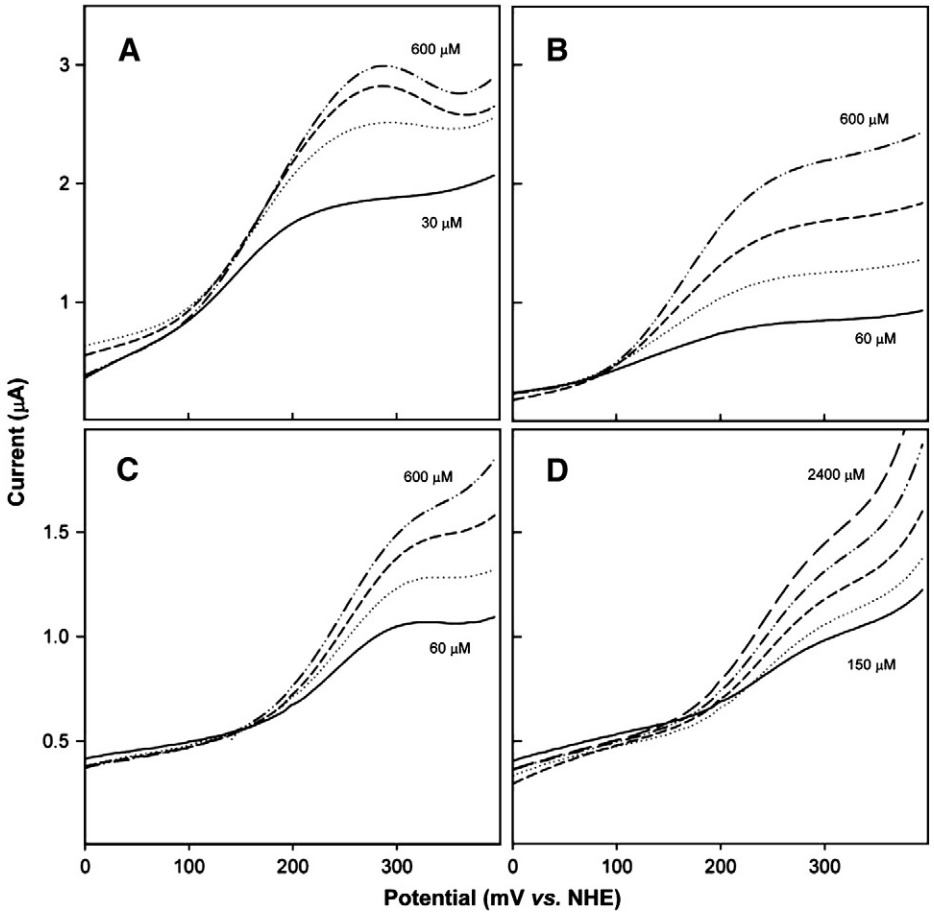

Fig. 8. The effect of sulfite concentration of the voltammetric waveform in wild type and substituted sulfite dehydrogenases: A – SDH^{WT} (pH 8.0), B – SDH^{R55K} (pH 8.0), C – SDH^{H57A} (pH 8.0), D – SDH^{R55M} (pH 6.0). Only the anodic sweeps are shown for clarity, but the cathodic sweep is in each case identical and only offset by the capacitive current. A scan rate of 5 mV s^{-1} and a rotation rate of 500 rpm were used throughout. Kanamycin films were used to stabilize the adsorbed enzyme for all except panel D where a polylysine film was used.

Having eliminated all other possibilities, there must be a potential dependent change in catalytic activity coupled to a redox reaction on the enzyme. Similarly non-ideal voltammetric behavior has been seen in a number of Mo enzymes and a variety of models have been proposed in order to account for the observations [28,43,45–49]. All of these models employ a function that is a convolution of two sigmoidal waves (with different limiting currents), interconverted by a redox switch at E_{sw}. Eq. (8a) is a rearranged form of the equation reported by Heffron et al. to model the peak shaped voltammetry of *E. coli* DMSO reductase [28] with appropriate sign changes to reflect an anodic catalytic current. The catalytic half-wave potential E_{cat} and the switch potential E_{sw} define where catalysis commences and where it becomes attenuated. The values of i_{lim} and i'_{lim} ($i'_{lim}<i_{lim}$) represent the two limiting currents of the more and less electrochemically active forms, respectively (Eqs. (8c) and (8d)) limited by substrate turnover and IET respectively.

$$i = \frac{i'_{\mathrm{lim}} \times 10^{(E-E_{sw})/59} + i_{\mathrm{lim}}}{1 + 10^{(E-E_{sw})/59} + 10^{(E_{cat}-E)/59}} \tag{8a}$$

$$i = \frac{i_{\mathrm{lim}}}{1 + 10^{(E_{cat}-E)/59}} \tag{8b}$$

$$i_{\mathrm{lim}} = \frac{nFA\Gamma_{SDH}k_2\left[SO_3^{2-}\right]}{K_{M,echem} + \left[SO_3^{2-}\right]} \tag{8c}$$

$$i'_{\mathrm{lim}} = \frac{nFA\Gamma_{SDH}k_{IET2}\left[SO_3^{2-}\right]}{K_{M,echem} + \left[SO_3^{2-}\right]} \tag{8d}$$

The experimental voltammetry of SDH^{WT} at high sulfite concentration (300 μM) was modelled with Eq. (8a) (Fig. 9). Only the anodic sweep is shown (which is identical to the cathodic sweep offset by the charging current, see Fig. 2). From the fit to Eq. (8a), the following parameters were obtained: $E_{sw} = 360 \pm 10$ mV; $E_{cat} = 175 \pm 10$ mV and the ratio of $i'_{\mathrm{lim}}/i_{\mathrm{lim}} = 0.77$ (attenuation of the maximum current at high overpotential). At lower (non-saturating) sulfite concentrations (such as 30 μM, Fig. 9) no peak is apparent and the voltammogram may be modelled as a simple sigmoidal function (Eq. (8b)) where all terms involving E_{sw} have vanished. The value of E_{cat} (146 ± 5 mV) is not significantly different from that obtained from Eq. (8a) for the higher sulfite concentration experiment.

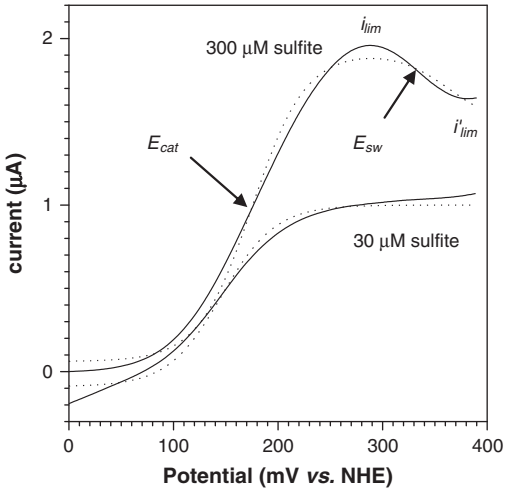

Fig. 9. Background subtracted experimental (solid lines) and calculated (dotted lines) voltammograms (anodic sweeps) at 300 μM (Eq. (8a)) and 30 μM sulfite (Eq. (8b)). Experimental conditions 500 rpm rotation rate, pH 8.0. The limiting currents i_{lim} and i'_{lim} are defined in Eqs. (8c) and (8d).

4.4. The physical significance of the E_{cat}, E_{sw}, i_{lim} and i'_{lim}

The parameters obtained from Eqs. (8a) and (8b) (E_{cat}, E_{sw}, i_{lim} and i'_{lim}) must have physical significance. The value of E_{cat} obtained from the model for SDH^{WT} matches that of its $Mo^{VI/V}$ couple which is consistent with heterogeneous electron transfer with the active site at low potential.

$$Mo^{VI} : Fe^{III} + SO_3^{2-} \xrightarrow{k_2} Mo^{IV} : Fe^{III} + SO_4^{2-} \xrightarrow{IET1} Mo^{V} : Fe^{II} \tag{9}$$

The value of E_{sw}, by elimination of all other redox centers, must correspond with the $Fe^{III/II}$ couple. Although the value of E_{sw} for SDH^{WT} obtained from fitting the data to Eq. (8a) is higher than the heme redox potential determined experimentally (Table 1), this variance is a reflection of the model and its constraints. Eq. (8a) has only 4 independent parameters (E_{cat}, E_{sw}, i_{lim} and i'_{lim}). We have assumed that the redox reactions (switching on catalysis at E_{cat} and switching to lower activity at E_{sw}) are each single electron process ($n = 1$). The n value determines the steepness of the rising part of the sigmoidal waveform and in this case it is affected by responses due to non-specific sulfite oxidation at high potential and trace oxygen reduction at low potential.

The magnitudes of i_{lim} and i'_{lim} are described using Eqs. (8c) and (8d). At low substrate concentrations, below or close to K_M, the current will be limited by the substrate concentration. At higher sulfite concentrations, where the enzyme is saturated, the current is limited by either k_2 (substrate turnover) or k_{IET2} (intramolecular electron transfer), through i_{lim} and i'_{lim} respectively. This means that at low sulfite concentrations (*e.g.* 30 μM, Fig. 9) $i_{lim} \approx i'_{lim}$ and no peak appears while at higher sulfite concentrations (300 μM, Fig. 9) $i_{lim} > i'_{lim}$ giving rise to a peak shaped voltammetric response. The values of both i_{lim} and i'_{lim} are proportional to the surface coverage of enzyme (Γ_{SDH}), which in this case was unknown without the observation of non-turnover responses from the cofactors in the absence of sulfite.

Evidence to support the fact that k_{IET2} is slower than k_2 can be found from two different experimental techniques; firstly the non-steady state parameters of the reductive half reaction of SDH^{WT} (Eq. (9)) have been determined using stopped flow techniques [13]. As shown, this comprises the reaction between SDH^{WT} (in its Mo^{VI}:Fe^{III} form) and sulfite forming the two-electron reduced Mo^{V}:Fe^{II} and sulfate as stable products. This overall process includes substrate binding, turnover and IET1 (Scheme 4B). For SDH^{WT} at pH 8, the values $k_{red} = 776\ s^{-1}$ *vs.* $k_{cat} = 345\ s^{-1}$ have been determined [13]. These results indicate that the rate limiting step is somewhere on the oxidative half cycle; either the second IET step (IET2 in Scheme 4B, corresponding to k_r in Eq. (6a)) or reaction with the cytochrome *c* acceptor. In the present case the cytochrome *c* partner has been substituted by the electrode and heterogeneous electron transfer is assumed to be non-rate limiting so the second IET step (Mo^{V} to Fe^{III}, IET2) emerges as the rate limiting step once the applied potential exceeds E_{sw}.

Secondly, k_{IET2} has been measured independently by laser flash photolysis [15]; *i.e.* k_r in Eq. (6a). One caveat is that in order to observe the Mo^{V}:$Fe^{III} \rightarrow Mo^{VI}$:$Fe^{II}$ IET reaction, the experiments were carried out at pH ~6 in order to raise the pH dependent $Mo^{VI/V}$ redox potential, using the established pH dependence of the $Mo^{VI/V}$ redox potential, so that an equilibrium between the Mo^{V}:Fe^{III} and Mo^{VI}:Fe^{II} results. Although direct comparisons with the kinetic data at pH 8 are not possible, the first order rate constant for the IET2 reaction (k_r) of SDH^{WT} was *ca.* $60\ s^{-1}$. This is an order of magnitude smaller than the data obtained for k_{red} and again supports the hypothesis that IET2 (Scheme 4B) is rate limiting.

The final question to be answered is why should electron transfer be diverted *via* the heme at all past the switch potential such that

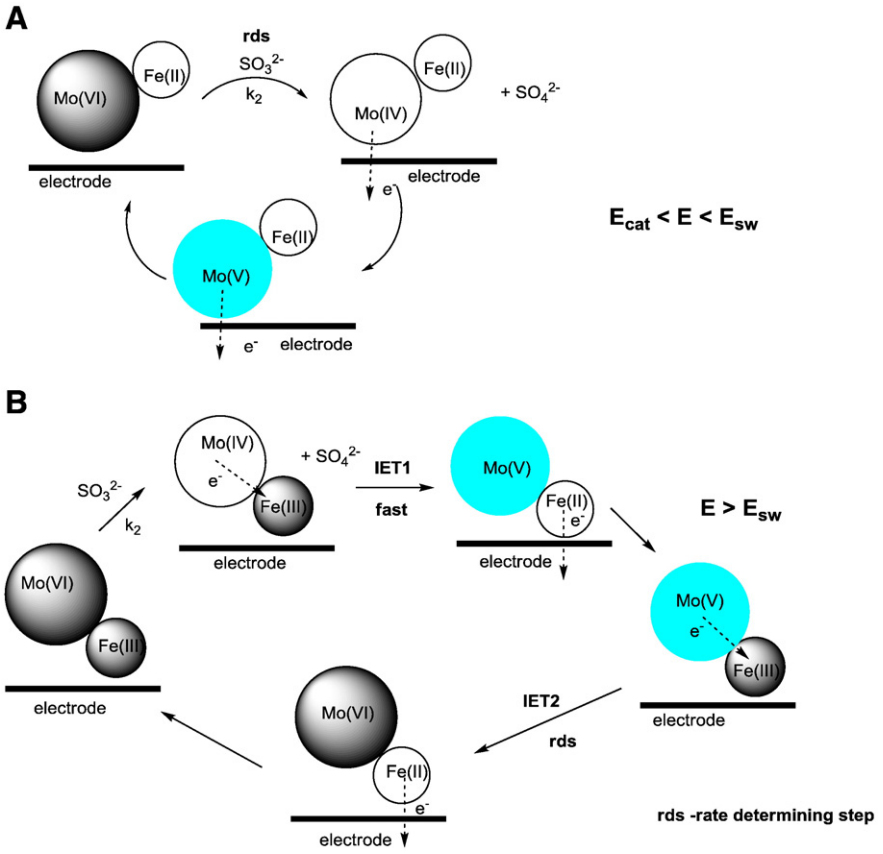

Scheme 4. (A) direct electron transfer with the Mo active site below E_{sw} and (B) electron transfer via the heme cofactor at high potential.

IET2 becomes rate limiting? We propose that the enzyme orientation at the electrode surface is altered in response to oxidation of the heme and heterogeneous electron transfer with the heme is switched on at the expense of the Mo active site. This is represented in cartoon form in Scheme 4B ($E>E_{sw}$) where the heme cofactor is shown to be closer to the electrode surface than the Mo active site and *vice versa* in Scheme 4A ($E<E_{sw}$). Although the enzyme is confined to the electrode surface, scanning probe microscopy studies of other proteins on graphite electrodes [50] have shown that their orientation is random and dynamic unless specifically anchored *via* a covalent link to the electrode surface. Reorientation of SDH^{WT} as the heme redox potential is approached is necessary so that heterogeneous electron transfer with the heme can take place and a Nernstian equilibrium is maintained. The key point is that given the crystal structure of SDH^{WT} shown in Fig. 10, it is unlikely that *both* the heme and Mo cofactors can *simultaneously* be close enough to the electrode to undergo heterogeneous electron transfer in parallel; it will be a case of one or the other so the switching model in Eq. (8a) is appropriate.

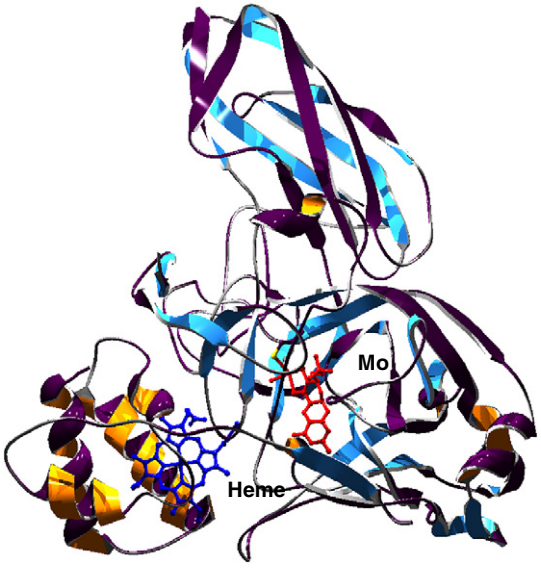

Fig. 10. Crystal structure SDH^{WT} [3] (coordinates taken from the Protein Data Bank, structure 2BLF) showing the positions of the Mo and heme cofactors. Structure manipulated with Swiss PDB Viewer (vers. 3.7) and rendered with PovRay (vers. 3.5).

5. Conclusions

Under physiological conditions, the heme *c* cofactor of SDH^{WT} is maintained in its ferric form by interactions with ferric cytochrome *c* in solution and thus is continuously poised to accept electrons from the Mo ion *via* intramolecular electron transfer (IET) (both Mo^{IV} to Fe^{III} and Mo^{V} to Fe^{III}). This is very different to a protein film voltammetry experiment where the oxidation states of the Mo and heme cofactors are altered in sequence according to their potentials. In SDH^{WT}, the heme cofactor is clearly the highest potential center so until the $Fe^{III/II}$ potential is reached during the anodic electrochemical sweep, the enzyme is locked into a state where IET (Mo^{V} to Fe^{II}) is blocked. However, a catalytic current is still observed at a potential (~175 mV) that is *well below* the heme redox potential (~240 mV). Therefore, heterogeneous electron transfer from Mo to the electrode must be occurring at potentials above E_{cat} and below E_{sw}, the heme cofactor is bypassed and the enzyme is effectively short-circuited as shown in Scheme 4A. As the potential is raised further ($E>E_{sw}$) the heme *c* cofactor is oxidized and IET is actuated. The drop in activity is due to IET being rate limiting current is lowered (Scheme 4B) and the cause of the switch

in electron transfer pathway is assigned to a change in enzyme orientation at the electrode surface. This is difficult to prove but we have no other explanation for the potential dependent lowering in activity beyond the potential of E_{sw}.

Turning to the substituted enzymes SDH^{H57A} and SDH^{R55M}, their lower heme redox potentials (which approach the $Mo^{VI/V}$ potential at pH 8) and the pH-independence of the catalytic potential indicates that electron transfer always proceeds *via* IET involving the heme *i.e.* there is no apparent switch within the range investigated. The remaining variant SDH^{R55K} has a similar pH dependent catalytic potential (Fig. 6) to the wild type enzyme suggesting that, for this substituted enzyme, electron transfer is occurring directly from the Mo center to the electrode. Previous kinetic measurements on SDH^{R55K} have found that its turnover number (k_{cat} 160 s^{-1} at pH 8 and 17 s^{-1} at pH 6) is about half that of the wild type enzyme [13]. The rate of IET2 has also recently been reported at pH 6 to be 15 s^{-1} which is not significantly different to k_{cat} at this pH [13]. Therefore, we propose that IET2 in SDH^{R55K} never becomes rate limiting ($k_2 < k_{IET2}$) so no drop in catalytic current is seen when the heme is oxidized. In all of the above variants (SDH^{H57A}, SDH^{R55M} and SDH^{R55K}), which are also much less active than SDH^{WT}, no peak shaped response is obtained and the current is limited by substrate turnover only.

Acknowledgements

PVB gratefully acknowledges grant support from the Australian Research Council (Discovery Project DP0880288) and UK acknowledges award of an ARC Australian Research Fellowship and grant (DP0878525). TDR thanks the University of Queensland for an International Postgraduate Research Scholarship.

References

[1] U. Kappler, Bacterial sulfite dehydrogenases — enzymes for chemolithtrophs only? in: C.G. Friedrich, C. Dahl (Eds.), Microbial Sulfur Metabolism, Springer, Berlin, 2007.
[2] R. Hille, Molybdenum enzymes, Essays Biochem. 34 (1999) 125–137.
[3] U. Kappler, S. Bailey, Molecular basis of intramolecular electron transfer in sulfite-oxidizing enzymes is revealed by high resolution structure of a heterodimeric complex of the catalytic molybdopterin subunit and a c-type cytochrome subunit, J. Biol. Chem. 280 (2005) 24999–25007.
[4] U. Kappler, S. Bailey, Crystallization and preliminary x-ray analysis of sulfite dehydrogenase from *Starkeya novella*, Acta Crystallogr., Sect D: Biol. Crystallogr. D 60 (2004) 2070–2072.
[5] R. Hille, The mononuclear molybdenum enzymes, Chem. Rev. 96 (1996) 2757–2816.
[6] R. Hille, Molybdenum enzymes containing the pyranopterin cofactor: an overview, Molybdenum and Tungsten: Their Roles in Biological Processes 39 (2002) 187–226.
[7] P.V. Bernhardt, Communicating with the mononuclear molybdoenzymes: emerging opportunities and applications in redox enzyme biosensors, in: J.J. Davis (Ed.), Engineering the Bioelectronic Interface:Applications to Analyte Biosensing and Protein Detection, Royal Society of Chemistry, 2009.
[8] C. Kisker, H. Schindelin, A. Pacheco, W.A. Wehbi, R.M. Garrett, K.V. Rajagopalan, J.H. Enemark, D.C. Rees, Molecular basis of sulfite oxidase deficiency from the structure of sulfite oxidase, Cell 91 (1997) 973–983.
[9] R.R. Mendel, F. Bittner, Cell biology of molybdenum, Biochim. Biophys. Acta Mol. Cell Res. 1763 (2006) 621–635.
[10] U. Kappler, B. Bennett, J. Rethmeier, G. Schwarz, R. Deutzmann, A.G. McEwan, C. Dahl, Sulfite:cytochrome c oxidoreductase from *Thiobacillus novellus*. Purification, characterization, and molecular biology of a heterodimeric member of the sulfite oxidase family, J. Biol. Chem. 275 (2000) 13202–13212.
[11] J.J. Wilson, U. Kappler, Sulfite oxidation in *Sinorhizobium meliloti*, Biochim. Biophys. Acta Bioenerg. 1787 (2009) 1516–1525.
[12] C.J. Feng, G. Tollin, J.H. Enemark, Sulfite oxidizing enzymes, Biochim. Biophys. Acta: Proteins Proteomics 1774 (2007) 527–539.
[13] S. Bailey, T. Rapson, K. Johnson-Winters, A.V. Astashkin, J.H. Enemark, U. Kappler, Molecular basis for enzymatic sulfite oxidation: how three conserved active site residues shape enzyme activity, J. Biol. Chem. 284 (2009) 2053–2063.
[14] U. Kappler, S. Bailey, C. Feng, M.J. Honeychurch, G.R. Hanson, P.V. Bernhardt, G. Tollin, J.H. Enemark, Kinetic and structural evidence for the importance of Tyr236 for the integrity of the Mo active site in a bacterial sulfite dehydrogenase, Biochemistry 45 (2006) 9696–9705.
[15] S. Emesh, T.D. Rapson, A. Rajapakshe, U. Kappler, P.V. Bernhardt, G. Tollin, J.H. Enemark, Intramolecular electron transfer in sulfite-oxidizing enzymes: elucidating the role of a conserved active site arginine, Biochemistry 48 (2009) 2156–2163.
[16] C. Leger, P. Bertrand, Direct electrochemistry of redox enzymes as a tool for mechanistic studies, Chem. Rev. 108 (2008) 2379–2438.
[17] P.V. Bernhardt, Enzyme electrochemistry — biocatalysis on an electrode, Aust. J. Chem. 59 (2006) 233–256.
[18] F.A. Armstrong, Recent developments in dynamic electrochemical studies of adsorbed enzymes and their active sites, Curr. Opin. Chem. Biol. 9 (2005) 110–117.
[19] K.-F. Aguey-Zinsou, P.V. Bernhardt, U. Kappler, A.G. McEwan, Direct electrochemistry of a bacterial sulfite dehydrogenase, J. Am. Chem. Soc. 125 (2003) 530–535.
[20] T.D. Rapson, U. Kappler, P.V. Bernhardt, Direct catalytic electrochemistry of sulfite dehydrogenase: mechanistic insights and contrasts with related Mo enzymes, Biochim. Biophys. Acta Bioenerg. 1777 (2008) 1319–1325.
[21] S.J. Elliott, A.E. McElhaney, C.J. Feng, J.H. Enemark, F.A. Armstrong, A voltammetric study of interdomain electron transfer within sulfite oxidase, J. Am. Chem. Soc. 124 (2002) 11612–11613.
[22] U. Kappler, A.G. McEwan, A system for the heterologous expression of complex redox proteins in *Rhodobacter capsulatus*: characterisation of recombinant sulphite:cytochrome c oxidoreductase from *Starkeya novella*, FEBS Lett. 529 (2002) 208–214.
[23] R. Codd, A.V. Astashkin, A. Pacheco, A.M. Raitsimring, J.H. Enemark, Pulsed ELDOR spectroscopy of the Mo(V)/Fe(III) state of sulfite oxidase prepared by one-electron reduction with Ti(III) citrate, J. Biol. Inorg. Chem. 7 (2002) 338–350.
[24] P.V. Bernhardt, K.-I. Chen, P.C. Sharpe, Transition metal complexes as mediator-titrants in protein redox potentiometry, J. Biol. Inorg. Chem. 11 (2006) 930–936.
[25] H.A. Heering, J. Hirst, F.A. Armstrong, Interpreting the catalytic voltammetry of electroactive enzymes adsorbed on electrodes, J. Phys. Chem. B 102 (1998) 6889–6902.
[26] C. Leger, S.J. Elliott, K.R. Hoke, L.J.C. Jeuken, A.K. Jones, F.A. Armstrong, Enzyme electrokinetics: using protein film voltammetry to investigate redox enzymes and their mechanisms, Biochemistry 42 (2003) 8653–8662.
[27] M.S. Brody, R. Hille, The kinetic behavior of chicken liver sulfite oxidase, Biochemistry 38 (1999) 6668–6677.
[28] K. Heffron, C. Leger, R.A. Rothery, J.H. Weiner, F.A. Armstrong, Determination of an optimal potential window for catalysis by *E. coli* dimethyl sulfoxide reductase and hypothesis on the role of Mo(V) in the reaction pathway, Biochemistry 40 (2001) 3117–3126.
[29] J.T. Spence, C.A. Kipke, J.H. Enemark, R.A. Sunde, Stoichiometry of electron uptake and the effect of anions and pH on the molybdenum and heme reduction potentials of sulfite oxidase, Inorg. Chem. 30 (1991) 3011–3015.
[30] E.E. Ferapontova, A. Christenson, A. Hellmark, T. Ruzgas, Spectroelectrochemical study of heme- and molybdopterin cofactor-containing chicken liver sulphite oxidase, Bioelectrochemistry 63 (2004) 49–53.
[31] C. Feng, U. Kappler, G. Tollin, J.H. Enemark, Intramolecular electron transfer in a bacterial sulfite dehydrogenase, J. Am. Chem. Soc. 125 (2003) 14696–14697.
[32] E.P. Sullivan Jr., J.T. Hazzard, G. Tollin, J.H. Enemark, Electron transfer in sulfite oxidase: effects of pH and anions on transient kinetics, Biochemistry 32 (1993) 12465–12470.
[33] A. Pacheco, J.T. Hazzard, G. Tollin, J.H. Enemark, The pH dependence of intramolecular electron transfer rates in sulfite oxidase at high and low anion concentrations, J. Biol. Inorg. Chem. 4 (1999) 390–401.
[34] C. Feng, R.V. Kedia, J.T. Hazzard, J.K. Hurley, G. Tollin, J.H. Enemark, Effect of solution viscosity on intramolecular electron transfer in sulfite oxidase, Biochemistry 41 (2002) 5816–5821.
[35] C.J. Feng, H.L. Wilson, G. Tollin, A.V. Astashkin, J.T. Hazzard, K.V. Rajagopalan, J.H. Enemark, The pathogenic human sulfite oxidase mutants G473D and A208D are defective in intramolecular electron transfer, Biochemistry 44 (2005) 13734–13743.
[36] L.A. Coury Jr., B.N. Oliver, J.O. Egekeze, C.S. Sosnoff, J.C. Brumfield, R.P. Buck, R.W. Murray, Mediated, anaerobic voltammetry of sulfite oxidase, Anal. Chem. 62 (1990) 452–458.
[37] L.A. Coury Jr., R.W. Murray, J.L. Johnson, K.V. Rajagopalan, Electrochemical study of kinetics of electron transfer between synthetic electron acceptors and reduced molybdoheme protein sulfite oxidase, J. Phys. Chem. 95 (1991) 6034–6040.
[38] L.A. Coury Jr., L. Yang, R.W. Murray, Electrochemical study of the rate of activation of the molybdoheme protein sulfite oxidase by organic electron acceptors, Anal. Chem. 65 (1993) 242–246.
[39] E.E. Ferapontova, T. Ruzgas, L. Gorton, Direct electron transfer of heme- and molybdopterin cofactor-containing chicken liver sulfite oxidase on alkanethiol-modified gold electrodes, Anal. Chem. 75 (2003) 4841–4850.
[40] R. Dronov, D.G. Kurth, H. Mohwald, R. Spricigo, S. Leimkuehler, U. Wollenberger, K.V. Rajagopalan, F.W. Scheller, F. Lisdat, Layer-by-layer arrangement by protein–protein interaction of sulfite oxidase and cytochrome c catalyzing oxidation of sulfite, J. Am. Chem. Soc. 130 (2008) 1122.
[41] R. Spricigo, R. Dronov, K.V. Rajagopalan, F. Lisdat, S. Leimkuehler, F.W. Scheller, U. Wollenberger, Electrocatalytically functional multilayer assembly of sulfite oxidase and cytochrome c, Soft Matter 4 (2008) 972–978.
[42] R. Spricigo, R. Dronov, F. Lisdat, S. Leimkuehler, F.W. Scheller, U. Wollenberger, Electrocatalytic sulfite biosensor with human sulfite oxidase co-immobilized with cytochrome c in a polyelectrolyte-containing multilayer, Anal. Bioanal. Chem. 393 (2009) 225–233.

[43] S.J. Elliott, C. Leger, H.R. Pershad, J. Hirst, K. Heffron, N. Ginet, F. Blasco, R.A. Rothery, J.H. Weiner, F.A. Armstrong, Detection and interpretation of redox potential optima in the catalytic activity of enzymes, Biochim. Biophys. Acta Bioenerg. 1555 (2002) 54–59.
[44] C. Leger, F. Lederer, B. Guigliarelli, P. Bertrand, Electron flow in multicenter enzymes: theory, applications, and consequences on the natural design of redox chains, J. Am. Chem. Soc. 128 (2006) 180–187.
[45] L.J. Anderson, D.J. Richardson, J.N. Butt, Using direct electrochemistry to probe rate limiting events during nitrate reductase turnover, Faraday Discuss. 116 (2000) 155–169.
[46] L.J. Anderson, D.J. Richardson, J.N. Butt, Catalytic protein film voltammetry from a respiratory nitrate reductase provides evidence for complex electrochemical modulation of enzyme activity, Biochemistry 40 (2001) 11294–11307.
[47] J.N. Butt, L.J. Anderson, L.M. Rubio, D.J. Richardson, E. Flores, A. Herrero, Enzyme-catalysed nitrate reduction-themes and variations as revealed by protein film voltammetry, Bioelectrochemistry 56 (2002) 17–18.
[48] S.J. Elliott, K.R. Hoke, K. Heffron, M. Palak, R.A. Rothery, J.H. Weiner, F.A. Armstrong, Voltammetric studies of the catalytic mechanism of the respiratory nitrate reductase from *Escherichia coli*: how nitrate reduction and inhibition depend on the oxidation state of the active site, Biochemistry 43 (2004) 799–807.
[49] B. Frangioni, P. Arnoux, M. Sabaty, D. Pignol, P. Bertrand, B. Guigliarelli, C. Leger, In Rhodobacter sphaeroides respiratory nitrate reductase, the kinetics of substrate binding favors intramolecular electron transfer, J. Am. Chem. Soc. 126 (2004) 1328–1329.
[50] J.J. Davis, H.A.O. Hill, The scanning probe microscopy of metalloproteins and metalloenzymes, Chem. Commun. (2002) 393–401.